SAND2019-3151R

Sandia National Laboratories

Operated for the U.S. Department of Energy
by National Technology and Engineering Solutions
of Sandia, LLC.

Albuquerque, New Mexico 87185
Livermore, California 94551

date: March 19, 2019

to: Distribution

from: B. T. Lester (1554), W. M. Scherzinger (1554)

subject: Modular Plane Stress Plasticity Material Model

1 Introduction

A variety of recent work has expanded capabilities in LAMÉ with respect to anisotropic and modular plasticity models (*e.g.* [1, 2, 3]). In this context, modular refers to a flexible framework and consistent implementation such that different hardening functional forms may all be incorporated into the same material model implementation rather than needing a new model for each description. However, such work has been focused on three-dimensional formulations and limited attention has been paid to structural formulations; *i.e.* for use with beam or shell elements. As a first step to bringing some of these recent advances towards structural elements, modular isotropic hardening capabilities will be added to the J_2, von Mises plane-stress plasticity formulation of Simo and Taylor [4].

To accomplish this effort, in Section 2 and 3 the theory and numerical formulation of the model are given. Specific functional forms of the hardening and example syntax to use them are then presented in Section 4 while verification exercises are documented in Section 5. Finally, some concluding thoughts about future work are given in Section 6.

2 Theory

The "Modular Plane Stress Plasticity" (MPSP) model is essentially the J_2 plane-stress model of Simo and Taylor [4] (also documented in Simo and Hughes [5]) with modified forms for the hardening. Specifically, kinematic hardening is neglected and the isotropic hardening is expanded to include rate-dependence and other recent advances in modularity.

In general, a J_2, von Mises effective stress measure, ϕ, may be written as,

$$\phi^2 = \frac{3}{2} s_{ij} s_{ij}, \qquad ; \qquad s_{ij} = \sigma_{ij} - \frac{1}{3}\sigma_{kk}\delta_{ij}, \tag{1}$$

in s_{ij} and σ_{ij} are the deviatoric and Cauchy stresses, respectively. Introducing the plane-stress assumption, $\sigma_{13} = \sigma_{23} = \sigma_{33} = 0$, the stress tensor has only three non-zero components. To go from three-dimensional descriptions to the plane-stress space, Simo and Taylor [4] introduce a projection matrix, $\underline{\underline{\bar{P}}}$,

$$\underline{\underline{\bar{P}}} = \frac{1}{3}\begin{bmatrix} 2 & -1 & 0 \\ -1 & 2 & 0 \\ 0 & 0 & 3 \end{bmatrix}, \tag{2}$$

such that,

$$\underline{s} = \underline{\underline{\bar{P}}}\,\underline{\sigma}, \tag{3}$$

with,

$$\underline{\sigma} = \begin{bmatrix} \sigma_{11} \\ \sigma_{22} \\ \sigma_{12} \end{bmatrix} \qquad ; \qquad \underline{s} = \begin{bmatrix} s_{11} \\ s_{22} \\ s_{12} \end{bmatrix}. \tag{4}$$

Note, in the preceding relations, and those that follow, matrix notation is used to directly represent variables in the projected plane-stress space to reinforce that the matrices are not tensors. A single underline ($\underline{x}$) is for arrays while a variable underlined twice ($\underline{\underline{X}}$) is a matrix.

In projected plane-stress space, the J_2, von Mises effective stress measure[1], $\bar{\phi}$, may be written,

$$\bar{\phi}^2 = \underline{\sigma}^T \underline{\underline{P}}\,\underline{\sigma}, \tag{5}$$

where a superscipt T denotes transpose and,

$$\underline{\underline{P}} = \frac{1}{3}\begin{bmatrix} 2 & -1 & 0 \\ -1 & 2 & 0 \\ 0 & 0 & 6 \end{bmatrix}. \tag{6}$$

[1]Note, with the projected plane-stress effective stress measure (Eqn. 5), a slight difference may be noted versus the typical, three-dimensional form (Eqn. 1) associated with with the leading constant. This arises from subtle differences in notation between the plane-stress references [4, 5] and the typical three-dimensional forms. The difference is accounted for in the forthcoming introduction of the yield surface radius, R, and the resulting yield functions are equivalent.

The yield function is then given as,

$$f = \bar{\phi}^2 \left(\sigma_{ij}\right) - R^2 \left(\bar{\varepsilon}^{\mathrm{p}}, \dot{\bar{\varepsilon}}^{\mathrm{p}}\right), \tag{7}$$

with R being the yield surface radius in the deviatoric π-plane and encapsulates the effects of isotropic hardening and $\bar{\varepsilon}^{\mathrm{p}}$ and $\dot{\bar{\varepsilon}}^{\mathrm{p}}$ are the equivalent plastic strain (isotropic hardening variable) and its rate. Note, models like Johnson-Cook [6, 7] also include temperature dependencies on the isotropic hardening. While such effects may be incorporated at a later date, for the moment they are neglected. The radius may be written in terms of the current yield stress, $\bar{\sigma}$, as,

$$R = \sqrt{\frac{2}{3}} \bar{\sigma} \left(\bar{\varepsilon}^{\mathrm{p}}, \dot{\bar{\varepsilon}}^{\mathrm{p}}\right). \tag{8}$$

Reflecting the intended "modular" nature of the model, descriptions for the current yield stress range from rate-independent, linear hardening to the most general "decoupled flow stress" form that may be written,

$$\bar{\sigma} \left(\bar{\varepsilon}^{\mathrm{p}}, \dot{\bar{\varepsilon}}^{\mathrm{p}}\right) = \sigma_y^0 \hat{\sigma}_y \left(\dot{\bar{\varepsilon}}^{\mathrm{p}}\right) + K \left(\bar{\varepsilon}^{\mathrm{p}}\right) \hat{\sigma}_h \left(\dot{\bar{\varepsilon}}^{\mathrm{p}}\right), \tag{9}$$

in which σ_y^0 and K are the initial yield stress and isotropic hardening, respectively, while $\hat{\sigma}_y$ and $\hat{\sigma}_h$ are rate-dependent multipliers for the yield and hardening. Note, rate-independence corresponds to constant values for the multipliers of one. While the various options and their corresponding syntax for $\bar{\sigma}$, K, $\hat{\sigma}_y$, and $\hat{\sigma}_h$ will be discussed later, a large variety of functional dependencies may be incorporated into such a hardening expression.

3 Implementation

To numerically integrate the MPSP model presented in Section 2, a hypoelastic approach leveraging an elastic-predictor/inelastic-corrector scheme is used. Note, with the exception of treatment of the modular hardening and utilization of a line-search step, the following scheme is largely that of Simo and Taylor [4] and Simo and Hughes [5]. As a first step, given a total strain increment $\underline{d\varepsilon} = \underline{\dot{\varepsilon}} \Delta t$, with $\Delta t = t_{n+1} - t_n$ where t_{n+1} is the current time and t_n is the time at the previous (known) solution step, a trial stress may be calculated as,

$$\underline{\sigma}^{\mathrm{tr}} = \underline{\underline{\bar{C}}} \left[\underline{\varepsilon}_n + \underline{d\varepsilon} - \underline{\varepsilon}_n^{\mathrm{p}}\right], \tag{10}$$

with,

$$\underline{\underline{\bar{C}}} = \frac{E}{1-\nu^2}\begin{bmatrix} 1 & \nu & 0 \\ \nu & 1 & 0 \\ 0 & 0 & \frac{1-\nu}{2} \end{bmatrix}, \tag{11}$$

being the plane-stress elastic stiffness matrix while E and ν are the elastic modulus and Poisson's ratio, respectively. A trial yield function value assuming purely elastic deformation may then be evaluated as,

$$f^{\mathrm{tr}} = \bar{\phi}^2\left(\underline{\sigma}^{\mathrm{tr}}\right) - R^2\left(\bar{\varepsilon}^{\mathrm{p}}_n, 0\right). \tag{12}$$

If $f^{\mathrm{tr}} \leq 0$, the solution is elastic and the variables may be updated with $\underline{\sigma}_{n+1} = \underline{\sigma}^{\mathrm{tr}}$ and $\bar{\varepsilon}^{\mathrm{p}}_{n+1} = \bar{\varepsilon}^{\mathrm{p}}_n$. In the case of plastic deformation, $f^{\mathrm{tr}} > 0$ an inelastic correction must be performed returning the trial stress state to an admissible state. For J_2 plasticity, this is commonly referred to as the "radial return" algorithm which requires the solution of only one non-linear equation. In the current plane-stress case, the same "radial return" approach cannot be used. However, the inelastic correction problem may still be reduced to a single non-linear equation to be solved. Thus, the development of an implementation for the current model requires two steps: (*i*) reduction/identification to a single equation and (*ii*) a numerical approach to solving it.

To address the first point, it is noted that the plastic strain tensor and equivalent plastic strain may be integrated (in a backward Euler fashion) as,

$$\underline{\varepsilon}^{\mathrm{p}}_{n+1} = \underline{\varepsilon}^{\mathrm{p}}_n + \lambda \underline{\underline{P}}\,\underline{\sigma}_{n+1}, \tag{13}$$

$$\bar{\varepsilon}^{\mathrm{p}}_{n+1} = \bar{\varepsilon}^{\mathrm{p}}_n + \lambda\sqrt{\frac{2}{3}}\bar{\phi}_{n+1}, \tag{14}$$

in which λ is the consistency multiplier. It is emphasized that because Eqn. 7 is second order the consistency multiplier and equivalent plastic strain increment are different quantities. Noting that the updated stress, $\underline{\sigma}_{n+1}$, may be written,

$$\underline{\sigma}_{n+1} = \underline{\underline{\bar{C}}}\left(\underline{\varepsilon}_{n+1} - \underline{\varepsilon}^{\mathrm{p}}_{n+1}\right), \tag{15}$$

which, by using Eqns. 10 and 13 and rearranging results in,

$$\left[\underline{\underline{I}} + \lambda \underline{\underline{\bar{C}}}\,\underline{\underline{P}}\right]\underline{\sigma}_{n+1} = \underline{\sigma}^{\mathrm{tr}}, \tag{16}$$

in which $\underline{\underline{I}}$ is the identity matrix.

As discussed more completely in Simo and Taylor [4], the plane-stress projection, $\underline{\underline{P}}$, and elasticity matrix, $\underline{\underline{\bar{C}}}$, share characteristic subspaces, $\underline{\underline{Q}}$, enabling them to be decomposed as,

$$\underline{\underline{P}} = \underline{\underline{Q}}\,\underline{\underline{\Lambda}}^{\mathrm{P}}\underline{\underline{Q}}^{T}, \qquad ; \qquad \underline{\underline{\bar{C}}} = \underline{\underline{Q}}\,\underline{\underline{\Lambda}}^{\mathrm{C}}\underline{\underline{Q}}^{T}, \tag{17}$$

with,

$$\underline{\underline{Q}}^{T} = \frac{1}{\sqrt{2}}\begin{bmatrix} 1 & 1 & 0 \\ -1 & 1 & 0 \\ 0 & 0 & \sqrt{2} \end{bmatrix} \;\; ; \;\; \underline{\underline{\Lambda}}^{P} = \begin{bmatrix} \frac{1}{3} & 0 & 0 \\ 0 & 1 & 0 \\ 0 & 0 & 2 \end{bmatrix} \;\; ; \;\; \underline{\underline{\Lambda}}^{C} = \begin{bmatrix} \frac{E}{1-\nu} & 0 & 0 \\ 0 & 2\mu & 0 \\ 0 & 0 & \mu \end{bmatrix}. \tag{18}$$

Introducing a transformed stress, $\underline{\eta}$, such that,

$$\underline{\eta} = \underline{\underline{Q}}^{T}\underline{\sigma}, \tag{19}$$

allows Eqn. 16 to be rewritten,

$$\left[\underline{\underline{I}} + \lambda\underline{\underline{\Lambda}}^{C}\underline{\underline{\Lambda}}^{P}\right]\underline{\eta}_{n+1} = \underline{\eta}^{\mathrm{tr}}. \tag{20}$$

It can be noted that from previous relations, the premultiplying matrix of Eqn. 20 is diagonal allowing for easy and analytic inversion.

Importantly, by inverting the matrix in Eqn. 20 the updated tranformed stress, $\underline{\eta}_{n+1}$, may be written in terms of the trial value (a known value) and a single unknown – the consistency multiplier. Thus, by inverting Eqn. 19, substituting into Eqn. 5, and using Eqn. 20, the effective stress $\bar{\phi}_{n+1}$ may be written as a function of λ alone as,

$$\bar{\phi}^{2}(\lambda) = \frac{\frac{1}{3}\left(\eta_{11}^{\mathrm{tr}}\right)^{2}}{\left[1+\lambda\frac{E}{3(1-\nu)}\right]^{2}} + \frac{\left(\eta_{22}^{\mathrm{tr}}\right)^{2} + 2\left(\eta_{12}^{\mathrm{tr}}\right)^{2}}{\left[1+\lambda 2\mu\right]^{2}}. \tag{21}$$

Furthermore, from Eqn. 14 it is observed that the updated value of the equivalent plastic strain, $\bar{\varepsilon}^{\mathrm{p}}_{n+1}$ is solely a function of λ such that,

$$\bar{\varepsilon}^{\mathrm{p}}_{n+1} = \bar{\varepsilon}^{\mathrm{p}}_{n} + \lambda\sqrt{\frac{2}{3}}\bar{\phi}_{n+1}(\lambda), \tag{22}$$

and the equivalent plastic strain rate, $\dot{\bar{\varepsilon}}^{\mathrm{p}}$, may be approximated as,

$$\dot{\bar{\varepsilon}}^{\mathrm{p}}(\lambda) \approx \frac{\bar{\varepsilon}^{\mathrm{p}}_{n+1} - \bar{\varepsilon}^{\mathrm{p}}_{n}}{\Delta t} = \frac{\lambda}{\Delta t}\sqrt{\frac{2}{3}}\bar{\phi}_{n+1}(\lambda). \tag{23}$$

Thus, performing the return map involves enforcing the consistency equation at the updated time step and may be written in terms of a single unknown as,

$$f_{n+1}(\lambda) = \bar{\phi}^2_{n+1}(\lambda) - R^2(\lambda) = 0. \tag{24}$$

To numerically solve Eqn. 24 a line-search augmented Newton-Raphson scheme is used. Recent work with non-quadratic and/or anisotropic plasticity models [1, 2] has demonstrated improved robustness by adopting such an approach over a traditional Newton-Raphson scheme. To this end, Eqn. 24 is recast in residual form as,

$$r^f = f_{n+1}(\lambda) = 0, \tag{25}$$

and linearized such that,

$$r^f_{k+1} = r^f_k + \frac{df}{d\lambda}\Delta\lambda, \tag{26}$$

where "k" is used to denote non-linear correction iteration and $\Delta\lambda$ is the increment in the consistency multiplier. Enforcing that $r^f_{k+1} = 0$ leads to,

$$\Delta\lambda = \frac{-r^f_k}{\frac{df}{d\lambda}}. \tag{27}$$

The derivative may be simply evaluated as,

$$\frac{df}{d\lambda} = \frac{d}{d\lambda}\left(\bar{\phi}^2\right) - \frac{d}{d\lambda}\left(R^2\right), \tag{28}$$

with

$$\frac{d}{d\lambda}\left(\bar{\phi}^2\right) = -2\left[\frac{E}{3(1-\nu)}\frac{\frac{1}{3}\left(\eta^{\mathrm{tr}}_{11}\right)^2}{\left[1+\lambda\frac{E}{3(1-\nu)}\right]^3} + 2\mu\frac{\left(\eta^{\mathrm{tr}}_{22}\right)^2 + 2\left(\eta^{\mathrm{tr}}_{12}\right)^2}{\left[1+\lambda 2\mu\right]^3}\right]. \tag{29}$$

Given the modular and flexible nature of the isotropic hardening specification, the form of the derivative of the radius can vary from quite simple to more complex. With the general form given in Eqn. 9, the derivative may be written,

$$\frac{d}{d\lambda}\left(R^2\right) = \frac{4}{3}\left(\sigma_y^0\hat{\sigma}_y + K\hat{\sigma}_h\right)\left[\hat{\sigma}_h\frac{\partial K}{\partial\bar{\varepsilon}^{\mathrm{p}}}\frac{\partial\bar{\varepsilon}^{\mathrm{p}}}{\partial\lambda} + \frac{\partial\dot{\bar{\varepsilon}}}{\partial\lambda}\left(\sigma_y^0\frac{\partial\hat{\sigma}_y}{\partial\dot{\bar{\varepsilon}}^{\mathrm{p}}} + K\frac{\partial\hat{\sigma}_h}{\partial\dot{\bar{\varepsilon}}^{\mathrm{p}}}\right)\right], \tag{30}$$

in which,

$$\frac{\partial\bar{\varepsilon}^{\mathrm{p}}}{\partial\lambda} = \sqrt{\frac{2}{3}}\left(\phi + \lambda\frac{\partial\phi}{\partial\lambda}\right), \tag{31}$$

$$\frac{\partial\dot{\bar{\varepsilon}}^{\mathrm{p}}}{\partial\lambda} = \frac{1}{\Delta t}\sqrt{\frac{2}{3}}\left(\phi + \lambda\frac{\partial\phi}{\partial\lambda}\right), \tag{32}$$

based on the expressions given in Eqns. 22 and 23, respectively.

The preceding relations all pertain to using the Newton-Raphson method to identify a "step-direction" in terms of the solution variable, λ. A line-search augmentation pertains to introducing and finding a "step-size", $0 < \alpha \leq 1$, that sufficiently minimizes a merit function thereby avoiding bad increments and improving robustness. Details on general line-search methods may be found in [8, 9] and their application to plasticity modeling in Pérez-Foguet and Armero [10] or Scherzinger [1]. Note, $\alpha = 1$ corresponds to a traditional Newton-Raphson scheme. For the current problem, a scaled merit function, ψ, is introduced such that,

$$\psi\left(\lambda\right) = \frac{1}{2}\left(\frac{r^f\left(\lambda\right)}{\left(\sigma_y^0\right)^2}\right)^2, \tag{33}$$

with $\left(\sigma_y^0\right)^2$ introduced as a scaling term (see [2] for a discussion on the impact of scaling). If the full Newton-Raphson step ($\alpha = 1$) sufficiently reduces the merit function, that step is used to increment the state variable. Otherwise, a quadratic approximation to the merit function is constructed and used to find a updated value of α to enforce that the merit function is always decreasing thereby ensuring convergence.

4 Hardening Specification and Examples

The previous sections laid out the theory and numerical implementation of the MPSP model. However, the specific forms of the isotropic hardening functions were left undefined given the multiple possibilities with the current modular framework. In this section, the different functional representations are described and examples of usage and corresponding syntax are given. Specifically, Section 4.1 describes different rate-independent options while rate-dependent formulations are given in Section 4.2.

To use the MODULAR_PLANE_STRESS_PLASTICITY model, the general input syntax is given below. Reflecting the modular nature, there are nine different hardening models that may be selected. In an attempt to clearly and simply present the required syntax for each of the models, the requisite input of each model will be defined in the following sections along with definitions of the corresponding parameters.

```
BEGIN PARAMETERS FOR MODEL MODULAR_PLANE_STRESS_PLASTICITY

    YOUNGS MODULUS = E
    POISSONS RATIO = ν
    YIELD_STRESS   = σ_y^0

    HARDENING MODEL = LINEAR | POWER_LAW | VOCE | USER_DEFINED
                    | CUBIC_HERMITE_SPLINE
                    | JOHNSON_COOK | POWER_LAW_BREAKDOWN
                    | FLOW_STRESS | DECOUPLED_FLOW_STRESS
                    •
                    •
        hardening model specification
                    •
                    •
END PARAMETERS FOR MODEL MODULAR_PLANE_STRESS_PLASTICITY
```

4.1 Rate-Independent

Rate-independent isotropic hardening takes the simplest form and may generally be written,

$$\bar{\sigma}\left(\bar{\varepsilon}^{\mathrm{p}}\right) = \sigma_y^0 + K\left(\bar{\varepsilon}^{\mathrm{p}}\right). \tag{34}$$

Representations of this form have been long studied and a number of specific forms exist. Currently, three of the more common analytic expressions – linear (K^{lin}), power-law (K^{pl}), and Voce (K^{voce}) – have been implemented and their expressions are given in Eqns. 35-37. Note, Voce is also sometimes referred to as "saturation" given the decaying exponential nature.

$$\begin{aligned} K^{\mathrm{lin}} &= H'\bar{\varepsilon}^{\mathrm{p}}, & (35)\\ K^{\mathrm{pl}} &= A^{\mathrm{pl}}\left(\bar{\varepsilon}^{\mathrm{p}}\right)^{n^{\mathrm{pl}}}, & (36)\\ K^{\mathrm{voce}} &= A^{\mathrm{v}}\left(1-\exp\left(-n^{\mathrm{v}}\bar{\varepsilon}^{\mathrm{p}}\right)\right), & (37)\\ \bar{\sigma} &= \tilde{\sigma}^{\mathrm{ud}}\left(\bar{\varepsilon}^{\mathrm{p}}\right) = \sigma_y^0 + K^{\mathrm{ud}}\left(\bar{\varepsilon}^{\mathrm{p}}\right). & (38) \end{aligned}$$

Additionally, Eqn. 38 indicates capabilities exist to use user-defined expressions (either in tabular or analytical form) to define isotropic hardening. However, Eqn. 38 also highlights

that some care must be taken in defining the corresponding function as different formulations may have slightly different interpretations. Specifically, in the rate-independent `USER_DEFINED` model, $\tilde{\sigma}^{\mathrm{ud}}(\bar{\varepsilon}^{\mathrm{p}})$ must be defined which includes both the constant initial yield stress and isotropic hardening. As such, $\tilde{\sigma}^{\mathrm{ud}}(0) = \sigma_y^0$. In rate-dependent models, however, either $\tilde{\sigma}^{\mathrm{ud}}(\bar{\varepsilon}^{\mathrm{p}})$ or $K^{\mathrm{ud}}(\bar{\varepsilon}^{\mathrm{p}})$ may be requested depending on the formulation. As indicated by Eqn. 38, the key difference between the two functions is that $K^{\mathrm{ud}}(\bar{\varepsilon}^{\mathrm{p}})$ incorporates isotropic hardening only. Therefore, $K^{\mathrm{ud}}(0) = 0$. To be clear, in what follows the two different functions will be used to explicitly indicate which should be used. Furthermore, $\tilde{\sigma}^{\mathrm{ud}}(\bar{\varepsilon}^{\mathrm{p}})$ is referred to as the `HARDENING FUNCTION` while $K^{\mathrm{ud}}(\bar{\varepsilon}^{\mathrm{p}})$ is denoted `ISOTROPIC HARDENING FUNCTION`. These functions are defined outside the material model definition block.

Example syntax for the different rate-independent models is given below.

```
 HARDENING MODEL = LINEAR
    HARDENING MODULUS = H'

HARDENING MODEL = POWER_LAW
    HARDENING CONSTANT= A^pl
    HARDENING EXPONENT= n^pl

HARDENING MODEL = VOCE
    HARDENING MODULUS= A^v
    EXPONENTIAL COEFFICIENT= n^v

HARDENING MODEL = USER_DEFINED
    HARDENING FUNCTION= σ̃^ud(ε̄^p)
```

4.2 Rate-Dependence

To incorporate rate-dependence, two different functional forms are considered. The first is the classic Johnson-Cook [6, 7] multiplier, $\hat{\sigma}^{\mathrm{jc}}$, while the second is referred to as "power-law breakdown", $\hat{\sigma}^{\mathrm{plb}}$. This latter form has been used with various models, notably that of Brown and Bammann [11], and detailed discussion of the motivation is left to that work. Expressions for these two models are given in Eqns. 39 and 40, respectively, in which C, $\dot{\varepsilon}_0$, g, and m are fitting coefficients.

$$\hat{\sigma}^{\mathrm{jc}} = 1 + C \ln\left(\frac{\dot{\bar{\varepsilon}}^{\mathrm{p}}}{\dot{\varepsilon}_0}\right), \tag{39}$$

$$\hat{\sigma}^{\mathrm{plb}} = 1 + \operatorname{asinh}\left(\left(\frac{\dot{\bar{\varepsilon}}^{\mathrm{p}}}{g}\right)^{1/m}\right). \tag{40}$$

As indicated by their expressions, $\hat{\sigma}^{\mathrm{jc}}$ and $\hat{\sigma}^{\mathrm{plb}}$ are referred to as rate multipliers as they take

a value on the order of 1 and scale the specified isotropic hardening function. In both cases, the rate-independent limit is one.

Hardening models for both `JOHNSON_COOK` and `POWER_LAW_BREAKDOWN` exist and may be specified as,

$$\bar{\sigma}\left(\bar{\varepsilon}^{\mathrm{p}}, \dot{\bar{\varepsilon}}^{\mathrm{p}}\right) = \tilde{\sigma}^{\mathrm{ud}}\left(\bar{\varepsilon}^{\mathrm{p}}\right) \hat{\sigma}^{\mathrm{jc,plb}}\left(\dot{\bar{\varepsilon}}^{\mathrm{p}}\right), \tag{41}$$

in which $\tilde{\sigma}^{\mathrm{ud}}$ is a user-defined hardening function. Example syntax for these models is given below.

```
HARDENING MODEL = JOHNSON_COOK
   HARDENING FUNCTION = σ̃^ud(ε̄^p)
   RATE CONSTANT= C
   REFERENCE RATE = ε̇_0

HARDENING MODEL = POWER_LAW_BREAKDOWN
   HARDENING FUNCTION = σ̃^ud(ε̄^p)
   RATE COEFFICIENT= g
   RATE EXPONENT = n
```

Flow Stress

`Flow_Stress` is the generic name of a hardening model that directly leverages the modular capabilities by assuming the form,

$$\bar{\sigma}\left(\bar{\varepsilon}^{\mathrm{p}}, \dot{\bar{\varepsilon}}^{\mathrm{p}}\right) = \left(\sigma_y^0 + K\left(\bar{\varepsilon}^{\mathrm{p}}\right)\right) \hat{\sigma}\left(\dot{\bar{\varepsilon}}^{\mathrm{p}}\right), \tag{42}$$

in which K and $\hat{\sigma}$ are a user-specified isotropic hardening and rate multiplier functions. The previously discussed `JOHNSON_COOK` and `POWER_LAW_BREAKDOWN` hardening models have very similar forms; the difference is the ability to analytically specify the isotropic hardening. As a first step to using this model, the forms of the isotropic hardening and rate multiplier must be specified via the below syntax.

```
HARDENING MODEL = FLOW_STRESS
   ISOTROPIC HARDENING MODEL = LINEAR | POWER_LAW | VOCE | USER_DEFINED
   RATE MULTIPLIER = JOHNSON_COOK | POWER_LAW_BREAKDOWN |
                     RATE_INDEPENDENT (RATE_INDEPENDENT)
```

Note, while the isotropic hardening model must be specified, the rate multiplier does not need to be specified. If the rate multiplier is left undefined, the response is taken to be rate independent and no further definition is needed. `RATE_INDEPENDENT` is also an acceptable

input enforcing that the rate multiplier takes a constant value of one. No additional input is needed for that option. To use the `LINEAR`, `POWER_LAW`, or `VOCE` isotropic hardening functions the corresponding parameters discussed in Section 4.1 must be defined. For the `USER_DEFINED`, however, an `ISOTROPIC HARDENING FUNCTION` is defined in lieu of `HARDENING FUNCTION`. This distinction is made to reinforce that $K^{\text{ud}}\left(\bar{\varepsilon}^{\text{p}}\right)$ needs to be provided instead of $\tilde{\sigma}^{\text{ud}}\left(\bar{\varepsilon}^{\text{p}}\right)$.

```
ISOTROPIC HARDENING FUNCTION = USER_DEFINED
       ISOTROPIC HARDENING FUNCTION = K^ud(ε̄^p)
```

With respect to the rate multipliers, while the names are the same as the hardening models their input syntax is slightly different. Namely, a hardening function does not need to be specified for their use. For clarity, the required parameters are repeated below.

```
RATE MULTIPLIER = JOHNSON_COOK
       RATE CONSTANT= C
       REFERENCE RATE = ε̇_0

RATE MULTIPLIER = POWER_LAW_BREAKDOWN
       RATE COEFFICIENT= g
       RATE EXPONENT = n
```

Decoupled Flow Stress

The `DECOUPLED_FLOW_STRESS` model essentially builds on the developments of the `FLOW_STRESS` capability to fully leverage the modular capabilities by allowing rate multipliers to be separately defined for the yield stress and isotropic hardening. The functional form was given previously in Eqn. 9. To use the `DECOUPLED_FLOW_STRESS` model the different functional forms must be specified. As with the `FLOW_STRESS` model, only the isotropic hardening model must be specified. If either (or both) of the rate multipliers are undefined, it is taken to be rate independent.

```
HARDENING MODEL = DECOUPLED_FLOW_STRESS
   ISOTROPIC HARDENING MODEL = LINEAR | POWER_LAW | VOCE | USER_DEFINED
   YIELD RATE MULTIPLIER = JOHNSON_COOK | POWER_LAW_BREAKDOWN |
                           RATE_INDEPENDENT (RATE_INDEPENDENT)
   HARDENING RATE MULTIPLIER = JOHNSON_COOK | POWER_LAW_BREAKDOWN |
                           RATE_INDEPENDENT (RATE_INDEPENDENT)
```

Specification of the `ISOTROPIC HARDENING MODEL` proceeds as discussed in the `FLOW_STRESS` section. Again, to be clear, if the `USER_DEFINED` option is used the required function to be input is $K^{\text{ud}}\left(\bar{\varepsilon}^{\text{p}}\right)$ and not $\tilde{\sigma}^{\text{ud}}\left(\bar{\varepsilon}^{\text{p}}\right)$. For the rate dependence, each multiplier must be defined as with the `FLOW_STRESS` model. Note, the key difference in this model is that a preceding

`YIELD` or `HARDENING` must be included to differentiate if the coefficient is with respect to $\hat{\sigma}_y\left(\dot{\bar{\varepsilon}}^{\mathrm{p}}\right)$ or $\hat{\sigma}_h\left(\dot{\bar{\varepsilon}}^{\mathrm{p}}\right)$. An example is given below.

```
 YIELD RATE MULTIPLIER = JOHNSON_COOK
        YIELD RATE CONSTANT= C
        YIELD REFERENCE RATE = ε̇_0

HARDENING RATE MULTIPLIER = POWER_LAW_BREAKDOWN
        HARDENING RATE COEFFICIENT= g
        HARDENING RATE EXPONENT = n
```

While the previous example used separate rate multipliers for yield and hardening there is no restriction in the formulation. If desired, the same rate multiplier models may be specified for the rate multipliers. Furthermore, even if the same model form is used, the associated model parameters do not need to be the same. It should be emphasized, however, that each rate multiplier and its corresponding properties must be specified separately. If the yield is defined but hardening is not, the hardening rate multiplier is taken to be rate independent and *vice versa*.

5 Verification

While the modularity of the MPSP model gives it some exciting possibilities, it does pose a slight complication for verification of the implementation. Specifically, covering all of the different combinations of hardening requires a large set of tests. To address this fact, more than 100 different hardening/loading tests have been conducted to ensure satisfactory performance of the implemented model. Here, a sampling of these tests are presented to demonstrate the verification process that has been undertaken and give some examples of results.

As all of the tests discussed here are for verification of the constitutive model, only one element was used. Additionally, only a single shell formulation was considered. The model parameters that were used for these verification tests are given in Table 1. "User-defined" hardening options were tested by defining a function equivalent to the Voce model. Given the similar responses, the "user-defined" results are omitted for clarity. Nonetheless, this functional capability was tested to the same extent as other hardening functions and the correct responses returned.

5.1 Uniaxial Stress

As a first verification step, the response of the model subject to a uniaxial tensile loading is investigated. In this case, the stress is assumed to take the form,

E	70 GPa	H'	500 MPa	C	0.1 (-)
ν	0.33 (-)	A^{pl}	400 MPa	$\dot{\varepsilon}_0$	1×10^{-4} s^{-1}
σ_y^0	200 MPa	n^{pl}	0.25 (-)	g	0.21 s^{-1}
		A^{v}	200 MPa	n	16.4 (-)
		n^{v}	20 (-)		

Table 1: Model parameters used for verification testing

$$\underline{\sigma}\left(t\right) = \begin{bmatrix} \sigma\left(t\right) \\ 0 \\ 0 \end{bmatrix}. \tag{43}$$

A two step test is considered in which a constant strain rate in the loading direction is applied. The first step is simply elastic loading and the total strain, $\varepsilon\left(t\right)$, may be taken to be $\varepsilon\left(t\right) = \dot{\bar{\varepsilon}}t$. Trivially, $\sigma\left(t\right) = E\dot{\bar{\varepsilon}}t$ and the time at the elastic limit (yield), t^{el}, is

$$t^{\mathrm{el}} = \frac{\sigma_y^0}{E\dot{\bar{\varepsilon}}}. \tag{44}$$

The second loading step corresponds to the elastic-plastic domain and a constant *equivalent plastic* strain rate is assumed such that $\dot{\bar{\varepsilon}}^{\mathrm{p}} = \dot{\bar{\varepsilon}}$. For convenience, $\dot{\bar{\varepsilon}}$ is taken to be the same both during the elastic and elastic-plastic steps. To determine the plastic strain rate in the loading direction, $\dot{\varepsilon}^{\mathrm{p}}$, the plastic work equivalency is considered. This expression may be given as,

$$\sigma_{ij}\dot{\varepsilon}_{ij}^{\mathrm{p}} = \bar{\sigma}\dot{\bar{\varepsilon}}^{\mathrm{p}}. \tag{45}$$

With the assumed uniaxial stress state, $\bar{\phi}^2 = \frac{2}{3}\sigma\left(t\right)$ and during plastic deformation $\bar{\phi}^2 = R^2$ leading to $\bar{\sigma} = \sigma\left(t\right)$. Using these observations and simplifying the plastic work equivalency with the known stress state leads to,

$$\sigma_{ij}\dot{\varepsilon}_{ij}^{\mathrm{p}} = \sigma\left(t\right)\dot{\varepsilon}^{\mathrm{p}} = \sigma\left(t\right)\dot{\bar{\varepsilon}}^{\mathrm{p}} \rightarrow \dot{\varepsilon}^{\mathrm{p}} = \dot{\bar{\varepsilon}}^{\mathrm{p}}. \tag{46}$$

Hooke's law may then be written as,

$$\sigma\left(t\right) = E\left(\varepsilon\left(t\right) - \varepsilon^{\mathrm{p}}\right), \tag{47}$$

which may be rearranged to write the total strain as,

$$\varepsilon\left(t\right) = \frac{\sigma\left(t\right)}{E} + \varepsilon^{\mathrm{p}}\left(t\right). \tag{48}$$

Noting the results of Eqn. 46 and the assumed constant plastic strain rate, $\varepsilon^{\mathrm{p}} = \bar{\varepsilon}^{\mathrm{p}} = \dot{\bar{\varepsilon}}\left(t - t^{\mathrm{el}}\right)$. With the equivalent plastic strain also known as a function of time, the current stress may simply be written as,

$$\sigma\left(t\right) = \bar{\sigma}\left(t\right) = \sigma_y^0 + K\left(\dot{\bar{\varepsilon}}\left(t - t^{\mathrm{el}}\right)\right), \tag{49}$$

yielding,

$$\varepsilon\left(t\right) = \frac{\sigma_y^0 + K\left(\dot{\bar{\varepsilon}}\left(t - t_{\mathrm{el}}\right)\right)}{E} + \dot{\bar{\varepsilon}}\left(t - t^{\mathrm{el}}\right). \tag{50}$$

With this result and the previous observation pertaining to the purely elastic stage, the total strain is known as a function of time. Thus, the corresponding displacement that may produce this result is simply,

$$u\left(t\right) = \exp\left(\varepsilon\left(t\right)\right) - 1. \tag{51}$$

Note, if yield is taken to be rate independent but hardening has rate dependence the same assumptions may be used to write the strain during plastic deformation as,

$$\varepsilon\left(t\right) = \frac{\sigma_y^0 + \hat{\sigma}_h\left(\dot{\bar{\varepsilon}}\right) K\left(\dot{\bar{\varepsilon}}\left(t - t_{\mathrm{el}}\right)\right)}{E} + \dot{\bar{\varepsilon}}\left(t - t^{\mathrm{el}}\right). \tag{52}$$

To verify the model performance, Fig. 1 presents the results determined analytically (denoted with an "(A)" in the legend) and numerically ("(N)") through finite element analysis for the rate-independent hardening forms. Clear agreement is noted in these cases between the various results. Additionally, some of the characteristic features of the different hardening models may be observed. Namely, the `linear` model has a linear slope during the elastic-plastic domain and the `Voce` response "saturates" and does not exhibit any additional hardening at sufficiently large plastic strains. The `power_law` hardening model, on the other hand, exhibits initial non-linearity but at larger strains exhibits a fairly linear slope.

To look at rate-dependent formulations, the `decoupled_flow_stress` model is used to test the results of Eqn. 52. Figure 2 presents the results of such a problem at two different strain rates using the `power_law_breakdown` model ; $\dot{\bar{\varepsilon}}^{\mathrm{p}} = 1 \times 10^{-3}$ s^{-1} in Fig. 2a and $\dot{\bar{\varepsilon}}^{\mathrm{p}} = 1$ s^{-1} in Fig. 2b. Similar tests were conducted with the `Johnson_Cook` model and exhibited comparable agreement but are not presented for brevity. Again clear agreement is noted between the analytical and numerical results and the impact of the rate is readily discernible by comparing the two result sets.

Next, the uniaxial stress problem is used to demonstrate the effect of the different rate multiplier combinations. To that end, Fig. 3 presents the results of a uniaxial stress problem

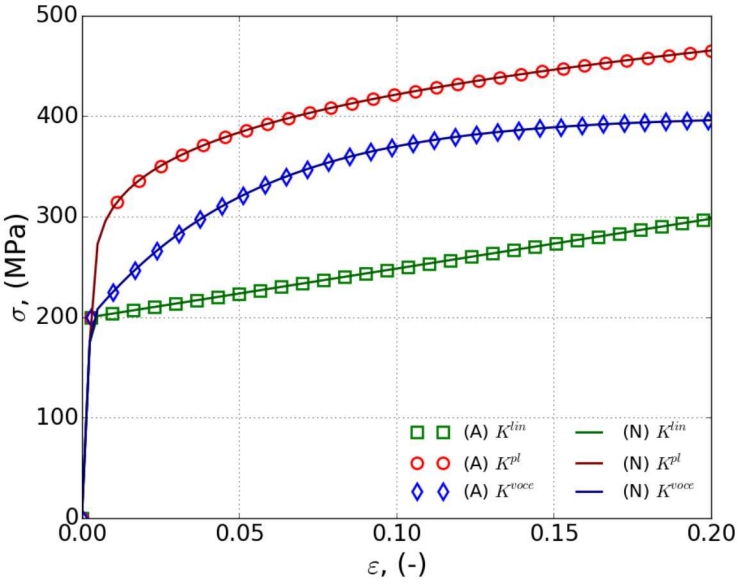

Figure 1: Analytical (A) and numerical (N) verification results of the rate-independent uniaxial stress problem considering different isotropic hardening functions.

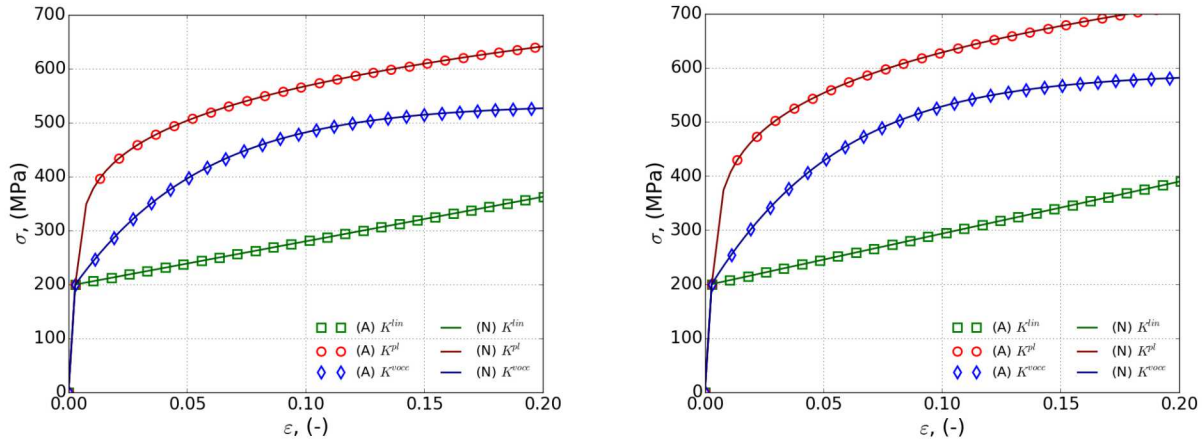

(a) $\dot{\bar{\varepsilon}} = 1 \times 10^{-3}$ s^{-1} (b) $\dot{\bar{\varepsilon}} = 1$ s^{-1}

Figure 2: Analytical (A) and numerical (N) verification results of the rate-dependent uniaxial stress problem with different isotropic hardening functions and constant strain rates of (a) $\dot{\bar{\varepsilon}} = 1 \times 10^{-3}$ s^{-1} and (a) $\dot{\bar{\varepsilon}} = 1$ s^{-1}.

with a constant *engineering* (not equivalent plastic) strain rate applied of $\dot{\bar{\varepsilon}}_{\text{eng}} = 1 \times 10^{-2}$ s^{-1}. The engineering rate is used instead of equivalent plastic to ensure a common strain path across the different problems. For the isotropic hardening, the user-defined functionality is used with a Voce like expression. The `decoupled_flow_stress` model is used to allow for

different descriptions of the rate multipliers. Different assumptions, either rate-independent or Johnson-Cook, are used for the rate multipliers to demonstrate the impact of each of the modular capabilities. From the results of Fig. 3 it is clear that having a rate multiplier on the constant yield stress will increase the apparent flow stress while having a hardening rate multiplier modifies (increases) the plastic hardening slope. Clearly, the biggest impact is in the Johnson-Cook like expression in which the rate multiplier acts on both terms.

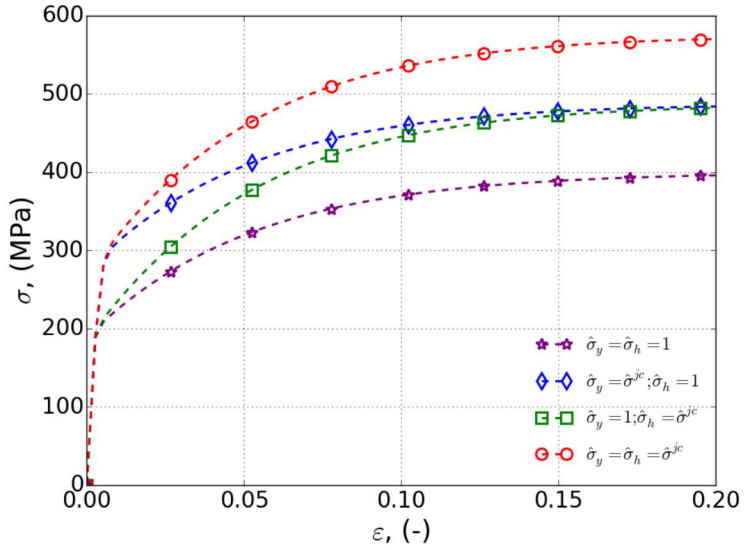

Figure 3: Stress-strain responses with a constant nominal strain rate $\dot{\varepsilon}_{\text{eng}} = 1 \times 10^{-2}\text{s}^{-1}$ with different Johnson-Cook rate multiplier selections.

5.2 Balanced Biaxial

For a second test, a balanced biaxial loading is considered. This problem has multiple stress components and, as will be seen in the next section, is equivalent to a pure shear solution in a rotated frame of reference. The current problem assumes a stress state of,

$$\underline{\sigma}\left(t\right) = \begin{bmatrix} \sigma\left(t\right) \\ -\sigma\left(t\right) \\ 0 \end{bmatrix}. \tag{53}$$

As with the uniaxial case, a two-step solution is pursued with an elastic step followed by an elastic-plastic step. A constant strain rate, $\dot{\bar{\varepsilon}}$, is considered during both stages. During the elastic step, it can be trivially shown that $\varepsilon_{11}\left(t\right) = -\varepsilon_{22}\left(t\right) = \dot{\bar{\varepsilon}}t$ and, after accounting for the Poisson effect,

$$\sigma\left(t\right) = 2\mu\dot{\bar{\varepsilon}}t. \tag{54}$$

For the assumed stress state, $\bar{\phi}^2 = 2\sigma^2(t)$ leading to an elastic limit time of,

$$t^{\text{el}} = \frac{\sigma_y^0}{2\sqrt{3}\mu\dot{\bar{\varepsilon}}}. \tag{55}$$

During plastic deformation, the equivalent plastic strain rate is taken to be constant, $\dot{\bar{\varepsilon}}^{\text{p}} = \dot{\bar{\varepsilon}}$, and, given the stress state, the plastic strain rate is assumed to be of the form,

$$\underline{\dot{\varepsilon}}^{\text{p}} = \begin{bmatrix} \dot{\varepsilon}^{\text{p}} \\ -\dot{\varepsilon}^{\text{p}} \\ 0 \end{bmatrix}, \tag{56}$$

in which it is clear that $\dot{\varepsilon}_{11}^{\text{p}} + \dot{\varepsilon}_{22}^{\text{p}} = 0 \rightarrow \dot{\varepsilon}_{33}^{\text{p}} = 0$ due to plastic incompressibility. The plastic work equivalency is then,

$$\sigma_{ij}\dot{\varepsilon}_{ij}^{\text{p}} = 2\sigma(t)\dot{\varepsilon}^{\text{p}} = \bar{\sigma}\dot{\bar{\varepsilon}}^{\text{p}} \rightarrow \dot{\varepsilon}^{\text{p}} = \frac{\sqrt{3}}{2}\dot{\bar{\varepsilon}}^{\text{p}}. \tag{57}$$

Finally, by decomposing the total strain such that,

$$\varepsilon(t) = \frac{\sigma(t)}{E} - \varepsilon^{\text{poisson}} + \varepsilon^{\text{p}}, \tag{58}$$

and rearranging using previous results,

$$\varepsilon(t) = \frac{1}{\sqrt{3}}\frac{\sigma_y^0 + \hat{\sigma}_h K\left(\dot{\bar{\varepsilon}}\left(t - t^{\text{el}}\right)\right)}{2\mu} + \frac{\sqrt{3}}{2}\dot{\bar{\varepsilon}}\left(t - t^{\text{el}}\right). \tag{59}$$

The desired material response may then be generated by applying a displacement of $u(t) = \exp(\varepsilon(t)) - 1$ in the tensile loading direction ("11") and $u(t) = \exp(-\varepsilon(t)) - 1$ in the compressive loading direction ("22").

Verification results of for this problem are presented in Fig. 4 for the rate-independent case. The positive values correspond to σ_{11} and compressive stresses are σ_{22}. Both are given as functions of the tensile strain, ε_{11}, for convenience. For the rate-dependent cases, the `power_law_breakdown` model is again used and results for constant strain rates of $\dot{\bar{\varepsilon}}^{\text{p}} = 1 \times 10^{-3}\text{s}^{-1}$ and $\dot{\bar{\varepsilon}}^{\text{p}} = 1\text{s}^{-1}$ are given in Figs. 5a and 5b, respectively.

In all cases, clear agreement is observed between the analytical ("(A)") and finite element (numerical "(N)") results. Importantly, agreement is observed for both the considered stress components verifying the capability of the implementation to handle multiaxial states of stress.

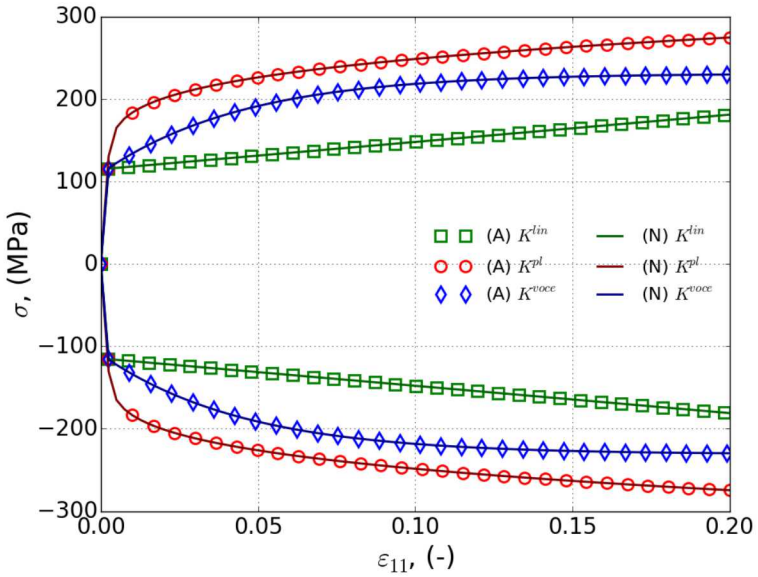

Figure 4: Analytical (A) and numerical (N) verification results of the rate-independent balanced biaxial stress problem considering different isotropic hardening functions. Positive results correspond to σ_{11} while the compressive results are for σ_{22}.

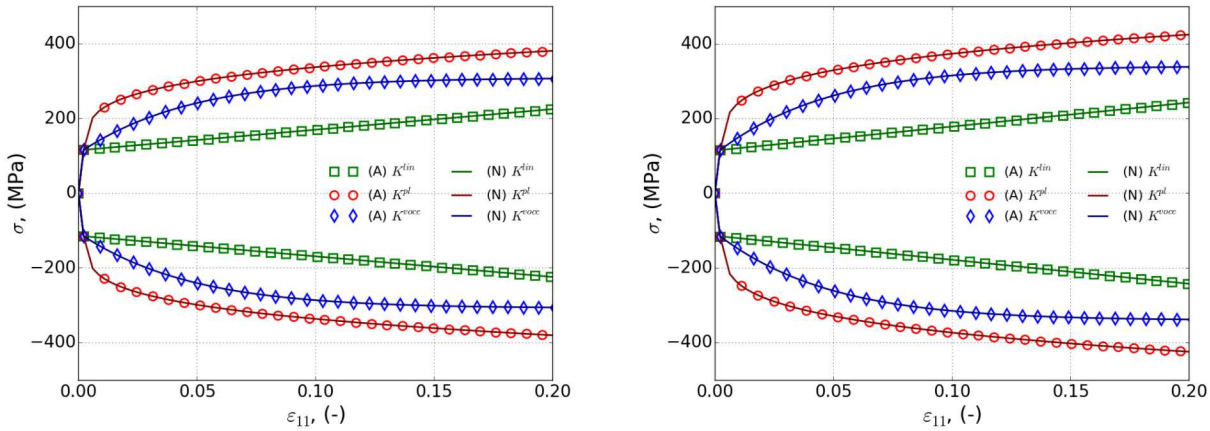

(a) $\dot{\bar{\varepsilon}} = 1 \times 10^{-3}$ s^{-1} (b) $\dot{\bar{\varepsilon}} = 1$ s^{-1}

Figure 5: Analytical (A) and numerical (N) verification results of the rate-dependent balanced biaxial stress problem with different isotropic hardening functions and constant strain rates of (a) $\dot{\bar{\varepsilon}} = 1 \times 10^{-3}$ s^{-1} and (a) $\dot{\bar{\varepsilon}} = 1$ s^{-1}. Positive results correspond to σ_{11} while the compressive results are for σ_{22}.

5.3 Biaxial Shear

For a final verification test, a problem which probes the shear response is desired. To that end, a stress state of,

$$\underline{\sigma}\left(t\right) = \begin{bmatrix} 0 \\ 0 \\ \sigma_{xy} \end{bmatrix}, \tag{60}$$

is assumed. In tensor form, it can also be trivially established that the balanced biaxial (Eqn. 53) and pure shear state (Eqn. 60) have the same principal stresses. Thus, a simple coordinate transformation of the problem should suffice to go from one to the other. This observation is also reinforced by the presence of the shear modulus, μ, in the various expressions of the balanced biaxial case rather than elastic modulus.

Therefore, to test the shear response, a rotated form of the balanced biaxial test is considered and will be referred to as "biaxial shear" for simplicity. To accomplish this task, the single element of the previous problems is rotated 45° about the out-of-plane direction. If the solution displacements of Section 5.2 are applied in the directions normal to the rotated model the desired pure shear stress state will result. Additionally, $\sigma_{xy}\left(t\right) = \sigma\left(t\right)$ from that same previous problem.

The results of these verification exercises are given in Fig. 6 for the rate-independent cases and Fig. 7 for rate-dependent instances with Figs. 7a and 7b presenting cases with $\dot{\bar{\varepsilon}}^{\mathrm{p}} = 1 \times 10^{-3}$ s^{-1} and $\dot{\bar{\varepsilon}}^{\mathrm{p}} = 1$ s^{-1}, respectively. As alluded to previously, the solution matches very closely with that of the previous balanced biaxial results and the analytical ("A") and numerical/finite element ("(N)") show excellent agreement.

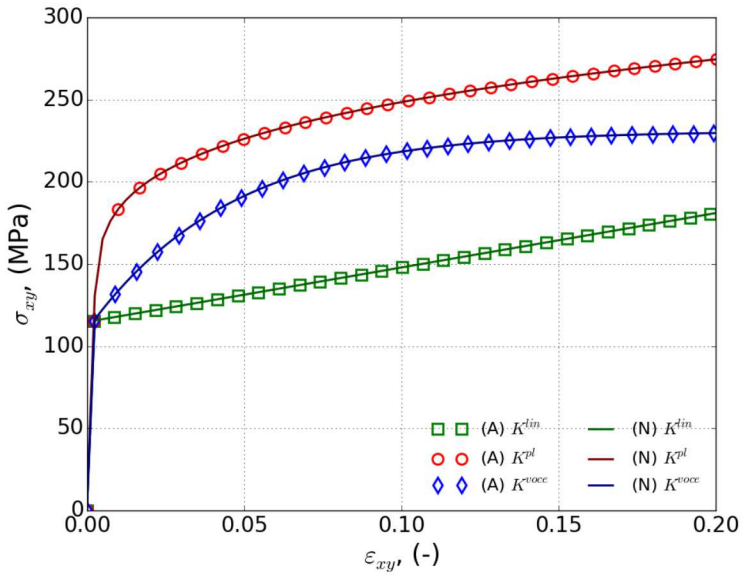

Figure 6: Analytical (A) and numerical (N) verification results of the rate-independent biaxial shear stress problem considering different isotropic hardening functions.

Importantly, although the test considers only one stress component it is the shear component.

Previous tests did not exercise the implementation of the model pertaining to the shear stress whereas this test does giving further credence to model performance.

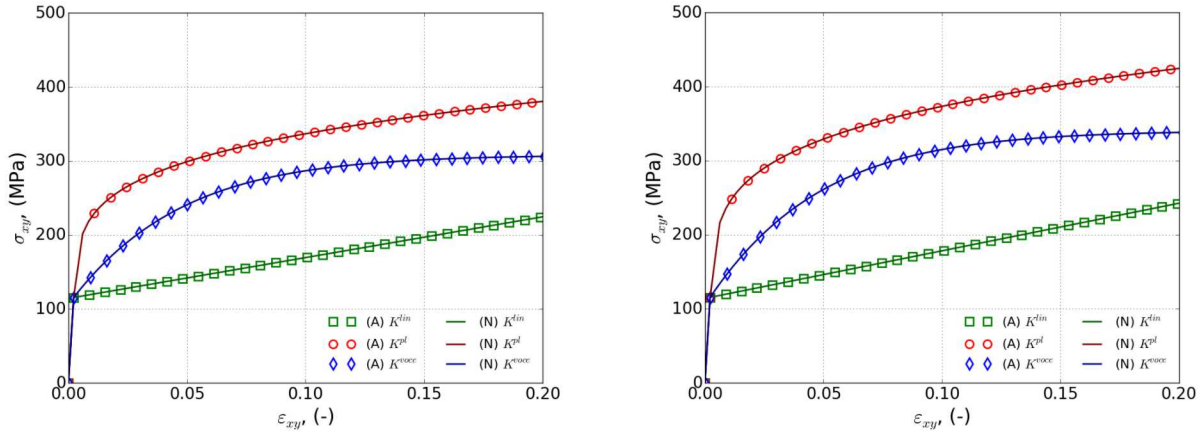

(a) $\dot{\bar{\varepsilon}} = 1 \times 10^{-3}$ s^{-1} (b) $\dot{\bar{\varepsilon}} = 1$ s^{-1}

Figure 7: Analytical (A) and numerical (N) verification results of the rate-dependent biaxial shear stress problem with different isotropic hardening functions and constant strain rates of (a) $\dot{\bar{\varepsilon}} = 1 \times 10^{-3}$ s^{-1} and (a) $\dot{\bar{\varepsilon}} = 1$ s^{-1}.

6 Conclusion

In this work, the `MODULAR_PLASTICITY_PLANE_STRESS` material model has been presented and discussed. Specifically, the considered model is a modified form of the J_2 plane-stress model of Simo and Taylor [4] incorporating recent improvements in modular, rate-dependent isotropic hardening and numerical implementation. To this end, the theory, numerical implementation, usage syntax, and examples have all been presented. The examples also served as verification exercises in which corresponding analytical solutions for the uniaxial stress, balanced biaxial, and biaxial shear were also determined and excellent agreement between the model and analytical results found.

Importantly, the developed model can also serve as a platform for additional extensions such as modular temperature dependence (*e.g.* Johnson-Cook [6] temperature multipliers), non-quadratic and/or anisotropic effective stress functions (*e.g.* the classic form of Hill [12]), different hardening forms (*e.g.* kinematic or distortional), or potentially failure models. Given the flexible form and robust implementation presented here, such additional capabilities could be readily integrated. Additionally, while verification exercises have been presented for the new model, model performance (*i.e.* speed) has not been investigated. Such considerations include both comparisons to other existing model forms as well as benchmarks against different combinations or specifications of hardening model in larger benchmark problems. These studies will be considered in the future.

Acknowledgements

Sandia National Laboratories is a multimission laboratory managed and operated by National Technology and Engineering Solutions of Sandia, LLC., a wholly owned subsidiary of Honeywell International, Inc., for the U.S. Department of Energy's National Nuclear Security Administration under contract DE-NA0003525. This paper describes objective technical results and analysis. Any subjective views or opinions that might be expressed in the paper do not necessarily represent the views of the U.S. Department of Energy or the United States Government.

Bibliography

[1] W. Scherzinger, A return mapping algorithm for isotropic and anisotropic plasticity models using a line search scheme, Computer Methods in Applied Mechanics and Engineering 317 (2017) 526–553.

[2] B. Lester, W. Scherzinger, Trust-region based return mapping algorithm for implicit integration of elastic-plastic constitutive models, International Journal for Numerical Methods in Engineering 112 (2017) 257–282.

[3] B. Lester, W. Scherzinger, An evolving effective stress approach to anisotropic distortional hardening, International Journal of Solids and Structures 143 (2018) 194–208.

[4] J. Simo, R. Taylor, A return mapping algorithm for plane stress elastoplasticity, International Journal for Numerical Methods in Engineering 22 (1986) 649–670.

[5] J. Simo, T. Hughes, Computational Inelasticity, Springer, New York, NY, 1998.

[6] G. Johnson, W. Cook, A constitutive model and data for metals subjected to large strains, high strain rates and high temperatures, in: Proc. 7$^{\text{th}}$ Int. Symp. on Ballistics, The Hague, The Netherlands, 1983, pp. 541–547.

[7] G. Johnson, W. Cook, Fracture characteristics of three metals subjected to various strains, strain rates, temperatures and pressures, Engineering Fracture Mechanics 21 (1) (1985) 31–48.

[8] D. G. Luenberger, Y. Ye, Linear and Nonlinear Programming, 3rd Edition, International Series in Operations Research and Management Science, Springer Science+Business Media, New York, NY, 2008.

[9] J. Nocedal, S. J. Wright, Numerical Optimization, 2nd Edition, Springer Series in Operations Research and Financial Engineering, Springer Science+Business Media, New York, NY, 2006.

[10] A. Pérez-Foguet, F. Armero, On the formulation of closest-point projection algorithms in elastoplasticity – part II: Globally convergent schemes, International Journal for Numerical Methods in Engineering 53 (2002) 331–374.

[11] A. Brown, D. Bammann, Validation of a model for static and dynamic recrystallization in metals, International Journal of Plasticity 32–33 (2012) 17–35.

[12] R. Hill, The Mathematical Theory of Plasticity, Claredon Press, Oxford, 1950.

Internal Distribution:

MS-0346 J. Bishop
MS-0346 A. Brink
MS-0346 K. Johnson
MS-0748 M. Starr
MS-0748 J. Wilkes
MS-0781 J. Bignell
MS-0790 C. Kirk
MS-0840 E. Corona
MS-0840 H. Fang
MS-0840 B. Lester
MS-0840 J. Rees
MS-0840 W. Scherzinger
MS-0840 D. Vangoethem
MS-0845 K. Pierson
MS-0845 J. Thomas
MS-9042 K. Karlson
MS-9042 S. Nelson
MS-9042 J. Ostien